Synthesis and in-vitro antibacterial properties of a functionally graded Ag impregnated composite surface

Ji, Xiaochao; Li, Xiaoying; Dong, Yangchun; Sammons, Rachel; Tian, Linhai; Yu, Helong; Zhang, Wei; Dong, Hanshan

DOI:
10.1016/j.msec.2019.01.087

Document Version
Peer reviewed version

Citation for published version (Harvard):
Ji, X, Li, X, Dong, Y, Sammons, R, Tian, L, Yu, H, Zhang, W & Dong, H 2019, 'Synthesis and in-vitro antibacterial properties of a functionally graded Ag impregnated composite surface', *Materials Science and Engineering C*, vol. 99, pp. 150-158. https://doi.org/10.1016/j.msec.2019.01.087

Synthesis and in-vitro antibacterial properties of a functionally graded Ag impregnated composite surface

Xiaochao Ji[a,d], Xiaoying Li[a], Yangchun Dong[a], Rachel Sammons[b], Linhai Tian[c], Helong Yu[d], Wei Zhang[e], Hanshan Dong[a]

[a]*School of Metallurgy and Materials, The University of Birmingham, Birmingham B15 2TT, UK*

[b]*School of Dentistry, The University of Birmingham, Birmingham, B5 7EG, UK*

[c]*Research Institute of Surface Engineering, Taiyuan University of Technology, Taiyuan 030024, China*

[d]*National Key Laboratory for Remanufacturing, AAAF, Beijing 100072, China.*

[e]*Jingjinji Institute of Remanufacturing Industry & Technology, Hebei 062450, China*

Abstract: Silver is considered promising in medical devices to prevent infection due to its excellent properties of broad antibacterial spectrum and persistent antibacterial activity. Herein, silver impregnated functionally graded composite surfaces have been developed by a novel duplex plasma deposition technique, which combines the double glow sputtering process and active screen plasma nitriding process. The composite surfaces include a surface antibacterial layer and a bottom supporting layer, which are deposited simultaneously. The functionally graded structure endows the composite surfaces with antibacterial activity, combined with improved wear resistance. The multilayer structures were observed by scanning electron microscopy, and the graded distribution of silver and nitrogen was verified by glow discharge optical emission spectroscopy. X-ray diffraction and X-ray photoelectron spectroscopy were used to analyze the microstructures and chemical states of the components. Results from

physical properties tests indicated that the composite surfaces have increased hardness, lower contact angles, excellent scratch resistance and wear resistance. The in-vitro antibacterial tests using the Gram-negative *E. Coli*. NCTC 10418 also showed that over 99% of bacteria were killed after 5h contacting with the composite surface.

Key words: antibacterial activity, silver, functionally graded coating, nitriding, active screen, stainless steel

1. INTRODUCTION

One significant problem encountered in metal medical devices is their weak resistance to the adhesion and growth of bacteria on their surfaces, which can cause cross contamination. The emergence of some superbugs such as Methicillin-resistant *Staphylococcus aureus* (MRSA) makes Hospital-Acquired Infections (HAIs) one of the chief causes of death all around the world. It is important to develop effective preventative technology to reduce bacterial adherence to the medical devices [1, 2]. Some inorganic antibacterial agents, such as silver, copper, calcium and titanium dioxide, have been reported to be effective in killing several disease-causing bacteria, including *E. coli*, *Staphylococcus aureus, Pneumococcus*, which can cause skin and wound infections [3-6]. However, bulk Ag or Cu are rarely used as hospital equipment metals due to their low strength and other shortcomings [7, 8]. Thus, concessional Ag or Cu containing coatings have been widely developed to improve the antibacterial properties of the medical devices [5, 9, 10].

Generally, medical devices such as surgical knives and scissors are made of stainless

steel (SS), which have high strength and excellent corrosion resistance. However, stainless steel has weak resistance to pathogens which may lead to nosocomial infections during surgery [11, 12]. Recent studies point to the development of long lasting antibacterial materials instead of conventional short-life cleaning agents. Silver is well known for its excellent antibacterial properties, such as inhibition of bacteria adhesion, broad anti-bacterial spectrum, and persistent anti-bacterial activity, because silver ions which dissociate from silver nanoparticles can kill various bacteria by damaging the cell walls [3]. Recently, several well-established techniques were employed to prepare the silver impregnated surfaces, such as plasma immersion ion implantation (PIII), physical vapor deposition (PVD), sol-gel method and so on [13-18]. PIII is able to implant Ag into different substrates like stainless steel, polyethylene, etc. but the implanted layers are very thin which may easily lose their antibacterial activity [13, 14]. PVD methods are able to fabricate thick antibacterial coatings. However, low hardness of the metal substrates will limit the improvement in wear resistance and result in short life [15, 16]. On the other hand, as silver is a noble metal, reducing the amount of silver without sacrificing antibacterial activity is essential for the practical applications of the composite surfaces. It is known that Ag impregnated composite surfaces have antibacterial activity, but a balance between the antibacterial efficacy and the amount of Ag should be considered in the design of the composite surfaces. Therefore, novel methods which can provide long lasting antibacterial coatings are desperately needed, and the correct percentage concentration of the doping Ag must be established.

Recently, a novel duplex plasma deposition technique, which combines the double glow plasma (DGP) process and the active screen plasma (ASP) alloying technique [19, 20], has been developed to fabricate wear and corrosion resistant composite surfaces with excellent antibacterial activity [21-23]. Properties of the functional composite surfaces are determined by the microstructures of the composite layers. These composite surfaces commonly contain an antibacterial agents impregnated composite coating layer and a superhard S-phase sublayer, which is a nitrogen interstitial supersaturated austenite layer [24]. The bio-functional surface layer provides antibacterial activity because of the antibacterial agents and the bottom S-phase layer shows excellent wear and corrosion resistance, which also provide good load bearing capacity due to its high hardness. Metallic medical devices as cardiovascular implants made by SS can undergo in vivo fretting damage which can enhance their susceptibility to pitting corrosion damage [25]. Pitting is typically initiated from the surface defects, which can be decreased due to the dense S-phase layer [26]. Thus, the functionally graded composite surfaces could be ideal structures as durable long-lasting antibacterial surfaces [19, 20]. However, as the duplex plasma deposition processes are combination of the sputtering process and the nitriding process, interferences between these two processes will influence the concentration of the antibacterial agents and the thickness of the S-phase layer, which have significant impacts on hardness, toughness and tribological properties of the composite surface.

The aim of this research was to develop functionally graded Ag impregnated composite surfaces, which were equipped with excellent wear resistance and

antibacterial performance by a novel duplex plasma deposition method. The influences of the duplex plasma deposition processes on the structure and properties of the composite surfaces were carefully studied. Various techniques were carried out to evaluate the morphologies, microstructure, chemical status, and mechanical properties of the as-deposited composite surfaces. Antibacterial tests were carried out to investigate the biodurability of these Ag impregnated composite surfaces.

2. MATERIALS AND METHODS

2.1 Materials and preparation

Commercial AISI 316 stainless steel were used as substrate with nominal composition (wt.%): 17.2 Cr, 11.7 Ni, 2.2 Mo, 1.3 Mn, 0.6 Si, 0.06 C, 0.026 P, 0.014 S, balance Fe. The dimensions of the samples were Ø25.4×5 mm with surface roughened by 1200 grit SiC paper. Samples were ultrasonically cleaned in acetone for 20 min and then dried prior to the deposition.

The duplex plasma processes were carried out with a DC plasma furnace (Klöckner 40 kW, Luxembourg) for the deposition of the functionally graded composite surfaces. Beside the DC power connected to the bottom electrode which controlled the voltage on the samples, an additional TruPlasma 3005 DC power source was installed to control the double glow plasma sputtering process, which was connected to the silver plate and the stainless-steel active screen. The schematic diagram of the settings is shown in Figure 1. Samples were placed on top of the bottom electrode and the silver plate and the stainless-steel active screen were connected to the additional TruPlasma 3005 DC power. The distance between the silver plate and the stainless-steel lid was

fixed at 15 mm. Other settings, sample codes and the deposition parameters are shown in Table 1. During the deposition, the gas mixtures were fed in to the chamber first, and then the main power source connected to bottom electrode was turned on to heat the chamber until 50℃ below the setting temperature. Then the additional power source is turned on for the deposition process.

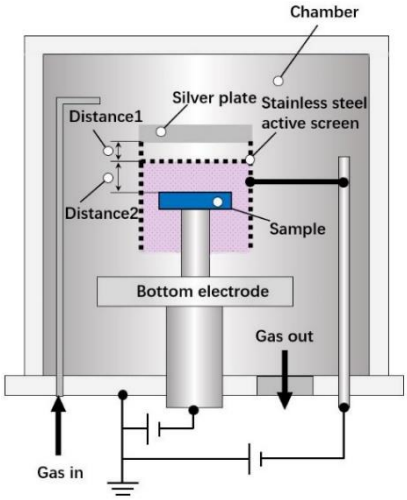

Figure 1 Schematic diagram of the settings of the duplex plasma treatment device for the deposition of the functionally graded Ag impregnated composite surface. Samples are placed on the working table which is connected to the bottom electrode. Targets are set on top of the samples which are connected to the additional power source.

Table 1 Sample codes and the duplex plasma treatment conditions, samples are deposited under different voltages and working distances.

Code	Substrate	Voltage		Distance 2	Pressure	Temperature	Gases		Time
		Bottom	Top				N_2	H_2	
S0	316SS	-	-	-	-	-	-	-	-
S1	316SS	200V	520V	25cm	1mbar	420℃	25%	75%	20h
S2	316SS	220V	510V	20cm	1mbar	420℃	25%	75%	20h
S3	316SS	240V	500V	15cm	1mbar	420℃	25%	75%	20h

2.2 Characterisation

Morphologies of the functionally graded coatings were observed by scanning electron microscopy (SEM, JEOL 7000) with energy dispersive spectroscopy (EDS) to investigate the elements distribution. All measurements were carried out at an

accelerating voltage of 20 kV. Glow discharge optical emission spectroscopy (GDOES, SPECTRUMA GDA650) was utilised to analyse the composition depth profile of the functionally graded coatings. X-ray diffraction (XRD) patterns of the samples were detected by a Bruker D8-Advanced diffractometer with Cu Kα radiation (λ=1.54056 Å). The patterns were analysed by X'Pert Highscore software with ICDD database 2004. X-ray photoemission spectroscopy (XPS, ESCALAB 250Xi, with Al Kα source) was used to investigate the chemical status of the Ag impregnated composite surface. Two etching cycles were carried out by the Ar ions to verify the chemical status consistence of the composite surfaces, and the time for each etching cycle was 60s. Microhardness was tested under a load of 50 g by a Vickers microhardness tester (Mitutoyo MVK-H1). Surface hydrophobicity was investigated with Biolin Scientific Theta contact angle meter. Distilled water (γ_{tot} = 72.8 mN m^{-1}, γ_d = 21.8 mN m^{-1}) was used and all measurements were carried out at 20℃.

2.3 Scratch and wear tests

Scratch testing on the surface of the functionally graded coatings was conducted with a Revetest scratch tester (CSM Instrument) with a Rockwell C diamond tip (radius 100 μm). The tip was drawn across the surface under a progressive load mode from 1 N to 10 N and the loading rate was 22.5 N/min. Scratch length was 2 mm at a speed of 5 mm/min. The normal load, tangential frictional force and acoustic emission signals were recorded during the tests. The friction tests were carried out with a reciprocating ball-on-plate CETR UMT-3 tribometer under wet conditions with Ringer's solution, which contains NaCl, KCL, $CaCl_2$ and $NaHCO_3$, similar to the

body fluid [27]. Friction parameters were 5 N at 5 Hz for 10min. The length of the wear tracks is 3 mm. Si_3N_4 ceramic balls (Ø 3.8mm) were used as the counterpart.

2.4 Antibacterial evaluation

The antibacterial tests were based on JIS Z 2801:2000 bacterial enumeration standard [28]. Polished untreated 316 stainless steel samples were used as control samples. Three samples from each deposition condition were tested and the average values were used to improve measurement precision. *E. coli* strain NCTC 10418 (Gram-negative) were used as test bacteria which were cultured in tryptone soya agar and then diluted in tryptone soya broth to an optical density of 0.05 (about 10^7 cells/ml). All samples were sterilised by autoclaving and then 50 ml diluted suspension (10^5 cells/ml) were pipetted onto the sample surface. A sterile glass coverslip was used to cover the suspension subsequently to keep equal contact area for the testing. Samples were then placed inside sterile 90 mm Petri dishes and then incubated at room temperature for a set time (5 h). The samples, together with the coverslips, were then transferred into a sterile container with 10 ml of sterile phosphate buffered saline (PBS) to dislodge the coverslip and suspend the bacteria from the sample with the aid of a vortex mixer. Each sample was agitated for 10 s. 100 µl aliquots of the diluted bacterial suspension were pipetted on Tryptone soya agar plates and incubated at 37℃ for 24 h (each sample 3 incubation). The number of the colony forming units (CFU) after incubation was counted by ImageJ, and each dot on the Petri dish was counted as one colony. The CFUs were used to evaluate the initial viability of the bacteria.

3. RESULTS AND DISCUSSION

3.1 Morphology

The duplex plasma deposition process combines the double glow plasma sputtering process and the active screen plasma nitriding process. The Ag and stainless-steel particles were sputtered on the substrates from the silver plate and the stainless-steel active screen lids to form the Ag impregnated layer. This co-sputtering was generated due to the hollow cathode effect between the Ag lid and the SS lid, dense plasma between two lids can significantly increase the sputter speed of metal particles. Meanwhile, the nitriding process was carried out, and the nitrogen ions can interact with the stainless-steel particles, which played a role in the transfer of nitrogen, and the diffusion process was carried out to form the S-phase due to the concentration gradient of nitrogen. In this case, the 'sputtering and deposition' mechanism can be applied to explain the formation of the S-phase, while the sputtered stainless-steel particles acted as nitrogen transfer agents [29]. Surface morphologies of the as-deposited functionally graded composite surfaces are shown in Figure 2 (a)&(b)&(c), whilst cauliflower-like surfaces are the results of the sputtering process. Some agglomerations can be viewed on the S1 sample, while the S2 and S3 composite surfaces are smoother.

Figure 2 (d)&(e)&(f) show the cross-sectional images of the functionally graded composite surfaces after etching by HCl + HNO_3 + H_2O (2:1:1) solution. Obvious interfaces between composite surface layer, S-phase sublayer and substrate can be distinguished. The thicknesses of the Ag impregnated composite layers are all about 2

μm, and thick S-phase layers were formed at the bottom of the coating layers, which show featureless morphologies, indicating the nitrogen supersaturated S-phase layer even can withstand the attack from acid solution. Thicknesses of the three samples are 13.5 μm (S1), 15.5 μm (S2), and 17.3 μm (S3), respectively. Etching craters can be viewed in the 316 SS substrates, which indicates the S-phase layer has better corrosion resistance compared to that of the 316 SS substrates. Confocal 3D images of the composite surfaces are shown in Figure 2 (g)&(h)&(i), and the average surface roughness (Ra) of S1, S2 and S3 varied with the deposition conditions, being 452 nm, 223 nm, and 124 nm, respectively.

The deposition process of the Ag impregnated layer was determined by top voltage, bottom voltage, and the sputtering distance. The higher the top voltage applied to the targets, the more and larger Ag and SS particles would be sputtered from the silver plate and the stainless-steel lid. Besides, the bottom voltage applied to the samples also caused a sputtering effect, which will remove some low energy particles, and benefit to form a dense coating [29, 30]. Forming of the composite surfaces were a result of the synergy between the two sputtering processes. It can be seen that S1 has a rougher surface and larger Ag particles are impregnated in the surface layer. Even though the sputtering distance of S3 was closer to the target than S1 and S2, the thicknesses of these three samples are similar due to the high bottom voltage applied to S3. Beside the large Ag particles, Ag nanoparticles were also formed during the sputtering process. The sputtered SS particles play an important role in transmitting of nitrogen in order to form the S-phase diffusion layer [29, 30].

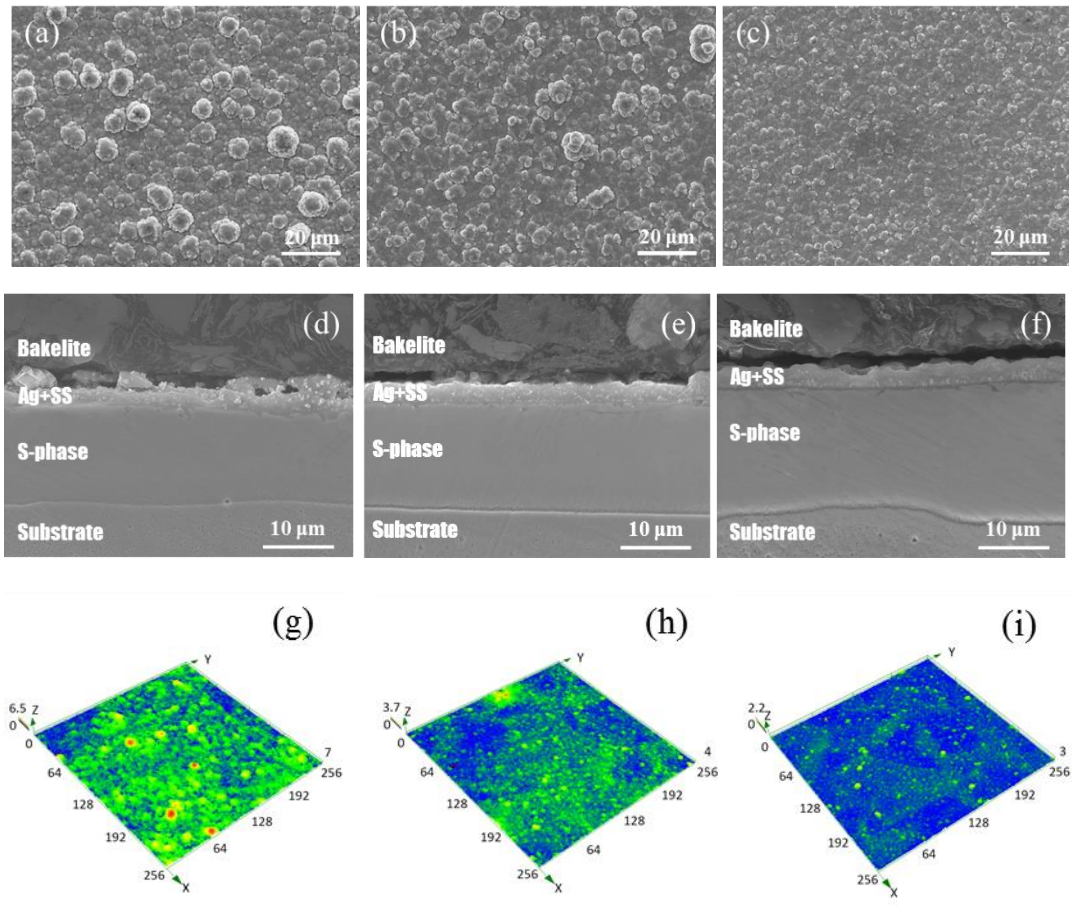

Figure 2 Surface morphologies, cross-sectional views and confocal 3D images of as deposited functionally graded composite surfaces: (a) large particles were accumulated on the surface of S1. (b) few large particles were formed during the sputtering process on S2. (c) relative smooth surface of S3. (d) cross-sectional view of S1 with obvious particles embedded in the coating. (e) clear interfaces can be distinguished from the cross-section view of S2. (f) dense coating layer and thick S-phase layer of S3. (g) 3D confocal morphologies of S1 while scale of the images is micrometers. (h) 3D images with less large particles on S2. (i) smooth surface of S3.

3.2 Depth profiles of silver and nitrogen

The distributions of silver and nitrogen in the composite surfaces are key to evaluate the antibacterial layer and the supporting S-phase layer. Figure 3(a) presents the depth profile of nitrogen and silver of the as-deposited composite surfaces measured by GDOES. The duplex plasma deposition process is a synergy of the sputtering process and the nitriding process. To some extent, the sputtered layer may interfere the nitrogen diffusion process as a barrier, leading to a graded distribution of nitrogen

within the composite coating and the S-phase layer. The composite surfaces show a similar decreasing trend of nitrogen from the surface to the substrate, while a higher descending slope of nitrogen can be observed within the composite coatings. Changing points of the nitrogen slopes can be recognised as the interfaces between coating/S-phase and S-phase/substrate. The results indicated that the sputtered layer would not inhibit the diffusion of nitrogen. The S1 sample presents lower nitrogen concentration in the S-phase layer compare to that of S2 and S3 samples, which may due to the long deposition distance and the interference of the large Ag particles [31].

The Ag depth profile can be used as a thickness indicator of the bio-functional layer. As shown in Figure 3(b) that the concentrations of Ag were affected by the deposition conditions, while the concentrations of Ag in the three composite coatings are 25 wt.% (S3), 13 wt.% (S2), and 5 wt.% (S1), respectively. Besides, all the Ag profiles illustrate a similar trend with two peak values at the surface and the interface. High percentage of Ag in S3 coating is mainly attributed to the short working distance, even though S1 and S2 were deposited under a higher sputtering voltage. The composite coatings were formed layer by layer during the co-sputtering process, and the high sputter rate of silver leads to the accumulation of Ag at initial and end stages of the sputtering process. The Ag rich surface layer is beneficial for the antibacterial reactions.

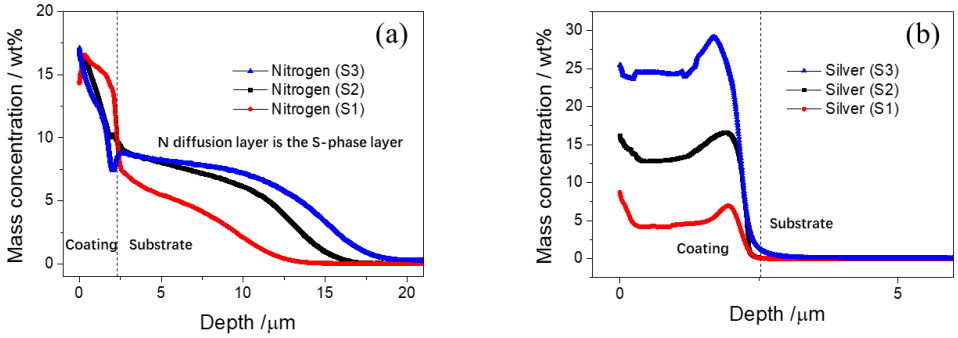

Figure 3 Depth profiles of (a) nitrogen and (b) silver in the composite surfaces, measured by glow discharge optical emission spectroscopy (GDOES). Nitrogen in the composite surfaces shows a graded descent trend from surface to substrate, which is existed in both the coating layer and the S-phase layer. Ag presents two peak concentration at the surface and interface area.

3.3 X-ray diffraction analysis

XRD results of the functionally graded composite and the untreated surfaces are shown in Figure 4. Typical γ(111), γ(200) and γ(220) were detected from the untreated surface, which confirm the face-centred cubic (fcc) structured austenitic stainless-steel substrate. XRD features detected from the composite surfaces are mainly related to Ag and stainless-steel. Peaks belong to pure Ag are clearly identified, whilst no features for Ag compounds are found, indicating there were not reactions between Ag in the plasma environment. Thus, no reduction of the antibacterial efficacy of the pristine Ag during the duplex plasma deposition process.

It was reported that the sputtered stainless-steel nanoparticles can react with nitrogen in the plasma environment, while Fe_xN particles are formed which act as nitrogen carriers. Due to the concentration gradient, nitrogen will desorb and then diffuse from the surface rich area into the substrate [29]. The saturated nitrogen atoms can cause lattice expansion within the stainless-steel which will induce the peak shift to left [32, 33], while the corresponding (111), (200) and (220) peaks cannot match that from the austenitic stainless-steel, and the peak (311) was observed at about 84^o due to the peak

shift. The variation of the peak intensity of Ag and S-phase is regarded to the concentration of Ag and stainless-steel. Composite surface with a high amount of Ag generates enhanced corresponding peaks, as well as the S-phase. Due to the relatively low deposition temperature (420℃), there was no chromium nitride precipitates were detected from the composite surfaces, indicating the duplex plasma deposition process has little influence on the corrosion resistance of the composite surface [34].

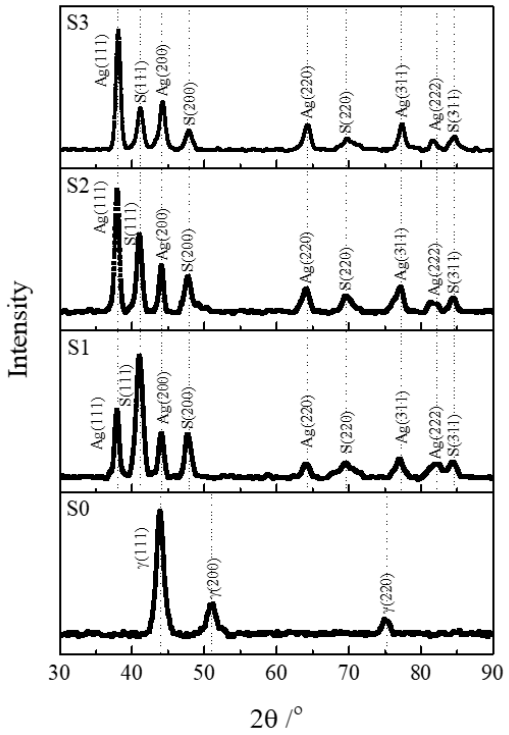

Figure 4 X-ray diffraction patterns of the untreated SS surface and the duplex plasma deposited functionally graded composite surfaces. S-phase and Ag are detected from all three composite surfaces while the intensities of these phases are influenced by their concentrations.

3.4 XPS analysis

XPS is sensitive to measure the elemental composition and chemical status of the extreme outer surface layer which interacts with the environment directly. In this study, the Ag impregnated composite surface was investigated by XPS to understand the chemical status of the surface that directly contacts the bacteria. High resolution

XPS spectra of Ag 3p, N 1s, Fe 2p and Cr 2p are shown in Figure 5. As can be seen, the spectra of all the three scans were matched well with each other, indicating that the chemical status of the near surface is uniform and stable. Two obvious peaks belonging to $Ag3d_{3/2}$ and $Ag3d_{5/2}$ can be found at 373.8 eV and 367.8 eV in the Ag 3p spectra, which are attributed to Ag and AgO, respectively. The appearance of AgO may due to the reaction between Ag and O_2 in the ambient air, and the thin layer of AgO was not detected by XRD. The N 1s spectra exhibits two pronounced peaks at 396.4 eV and 400.6 eV, which correspond to iron nitride and nitrogen [35, 36], respectively. Gammon et al. suggested that the component at 400.6 eV may come from N in a pyrrole-like configuration [37]. It is considered that some of the chemisorbed nitrogen atoms were reacted with Fe in the SS particles to form Fe_xN, while others were interstitial atoms and then diffused into the matrix to form the S-phase. Peaks for $Fe2p_{3/2}$ and $Fe2p_{1/2}$ can be found at 711.0 eV and 724.8 eV attributing to Fe^{3+} and Fe^{2+} [35], respectively. Indicating that iron nitrides Fe_2N or Fe_3N may accumulated on the composite surface. However, a weak peak at 706.7 eV attributed to Fe^0 can be distinguished in the Fe 2p spectra, which is due to the 'sputtering and deposition' mechanism of the formation of the S-phase [26]. SS particles were reacted with nitrogen during the sputtering process, whilst the desorbed nitrogen atoms were diffused into the deeper area to form S-phase. Chromium atoms substitute the lattice positions of iron atom in stainless steel and their valence states are accounted at zero. However, the XPS results indicate that the surface chromium atoms transferred into trivalent states [38], and two broad and week peaks located at

576.7 eV and 586.7 eV in the Cr 2p spectrum correspond to Cr $2p_{3/2}$ and Cr $2p_{1/2}$ of Cr^{3+} [39]. It means that the nitrogen plasma was reacted with both iron and chromium in the sputtered SS nanoparticles.

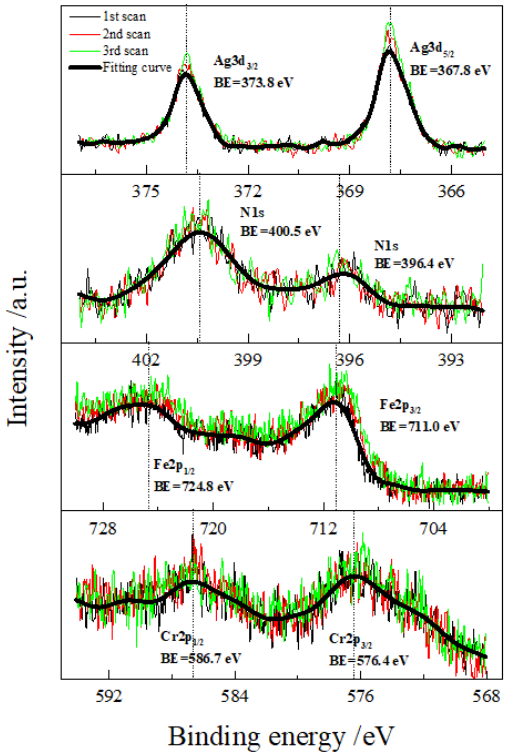

Figure 5 High resolution XPS spectra of Ag 3d, N 1s, Fe 2p and Cr 2p of Ag impregnated functionally graded composite coating. The three scans are closed to each other, indicating that chemical states of the surface layers are similar, while the spectra were fitted with the black lines.

3.5 Contact angle and microhardness

Wettability of the bio-functional surfaces can influence their contact with bacteria, which is correlated to the antibacterial efficiency. Typically, contact angle is applied to evaluate the wettability of a surface, which is determined by the chemical composition and its surface roughness. A surface is described as hydrophilic when its contact angle is lower than 90^{o} [40], to some extent, low contact angle can improve the aqueous dispersion which is beneficial for the contact between bacteria and the surfaces. As shown in Figure 6 that the contact angle of the polished SS surface is

about 96^{o} which is relatively hydrophobic, while the contact angles of the functionally graded composite surfaces are all around 60^{o}. This is because these surfaces are rich of nitrogen which can form a covalent bond with water. The hydrophilic surfaces tend to be more favourable to interact with the bacteria.

The results of micro hardness are illustrated in Figure 6. It is shown that hardness of the untreated stainless-steel sample is around 245 $HV_{0.05}$, which is much lower compared to the composite surfaces. The functionally graded composite surfaces are all equipped with high hardness due to the formation of the S-phase layer, which are about 682 $HV_{0.05}$ (S1), 820 $HV_{0.05}$ (S2), and 950 $HV_{0.05}$ (S3), respectively. The hard S-phase layer can provide high load bearing capacity for the composite surface layer to improve its wear resistance. Besides, the nitride stainless-steel nanoparticles are embedded in the composite coatings, which is also beneficial for the overall hardness. The S1 composite surface has the lowest hardness in the three composite surfaces, because it has the lowest concentration of nitrogen within the S-phase layer. Indicating that the diffusion of nitrogen plays an important role for hardness enhancement.

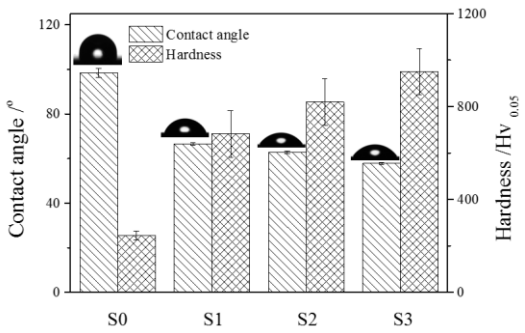

Figure 6 Contact angles and microhardness of the as-deposited functionally graded composite surfaces with the untreated substrate for comparison. The composite surfaces are equipped with high hardness

due to the formation of S-phase layer. The contact angles of the composite surfaces against water are smaller than that of the untreated stainless-steel surface which is benefit for the contact process.

3.6 Scratch resistance

Scratch testing was used to assess the quality and adhesion of the composite coating layer. In this study, the scratch resistance of the Ag impregnated surface layer is essential to keep its antibacterial function. Thus, the durability the coating was evaluated by progressively increasing load scratch tests from 1 N to 10 N. The normal load on the indenter is transferred to the front half of the tip and will cause bending of the coating. When the internal stress is sufficient, cracks tend to initiate at defect sites within the coating and then propagate to cause coating failure [41]. Figure 7(a) shows the applied normal load, recorded tangential load and acoustic emission signals during the scratch tests, and the insert image is a typical scratch track on S1. It can be seen that all three composite coatings presented excellent scratch resistance, while no obvious change of the slope of the tangential force during the progressive load scratch tests and no peeling off occurred. Acoustic emission signals were also recorded which detect the generation of cracks and can be used to evaluate the quality of the coating. The acoustic emission signals of S1 are higher than that of the S2 and S3, because more Ag particles were impregnated in S1 which may decrease the scratch resistance of the composite coating. As shown in Figure 7(b) that several tensile cracks can be found within the track while there is no buckling. It suggests the composite surfaces are very tough and equipped with excellent adhesion property [42].

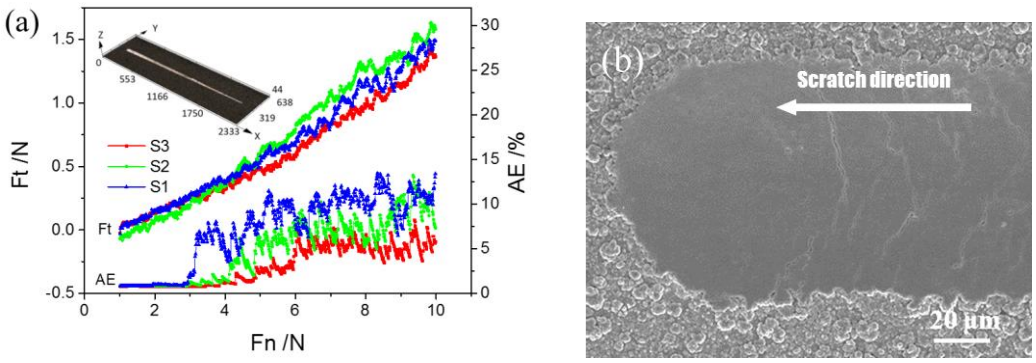

Figure 7 Scratch tests under progressive increasing load from 1N to 10N. (a) normal loads F_n, tangential loads F_t and acoustic emission signals during the scratch tests; the insert shows a 3D scratch track. (b) SEM image of the scratch track at the ending position on composite surface S1.

3.7 Wear resistance

Wear of bio-functional surfaces is inevitable during service and wear resistance is important for long-lasting antibacterial composite surfaces. Previous studies indicated that a hard S-phase layer can enhance the load bearing capacity of the composite surface and then improve the wear resistance under dry friction conditions [21-23]. In this study, the in-vitro study of the bio-functional composite surfaces was carried out within Ringer's solution to simulate the body fluid environment, and the load, frequency and time of the tests were 5 N, 5 Hz and 10 min, respectively.

Figure 8(a) shows the friction coefficient curves, while average friction coefficients of the three composite surfaces are 0.236 (S1), 0.242 (S2), and 0.224 (S3), respectively. Which are clearly lower than that of the stainless-steel surface (0.332) under the same tribological conditions. Meanwhile, the wear rate of the untreated stainless steel is around 363.9×10^{-8} mm^3/Nm, which is higher compared to that of the composite surfaces (74.7×10^{-8} mm^3/Nm (S1), 34.8×10^{-8} mm^3/Nm (S2), 48.1×10^{-8} mm^3/Nm (S3)), due the adhesive wear mode [43]. Wear tracks of the untreated surface (S0) and the composite surface (S1) are shown in Figure 9, and the EDS results of the selected

positions are shown in Table 2. Considering the ratio between Ag and Fe, the percentage of Ag was increasing in the damaged region (point 5). However, due to the reactions between the surface and oxygen, the decrease of the Ag content in the wear track area may reduce its antibacterial activity compared to that of the pristine coating. Rough surfaces with deeply scratched grooves and peeled-off craters were generated on the untreated stainless-steel surface due to the adhesive wear process even under the lubricant condition (See Figure 9(a)), while the wear tracks on the composite surface are more uniform and shallow scratched grooves indicate light abrasive mode of wear on the composite surfaces. The composite coating layer is formed by hard nitride stainless steel nanoparticles and soft Ag particles, which can reduce the generation of abrasives and prevent material transfer between the friction pair. Besides, the hard S-phase sublayer provides high load bearing capacity for the composite surface which also plays a key role in the improvement of wear resistance. On the other hand, Ringer's solution also acted as a corrosive agent during the friction tests. However, no corrosion happened on the composite surface after the friction tests due to the low temperature nitriding process, which avoids precipitation of chromium nitrides [26].

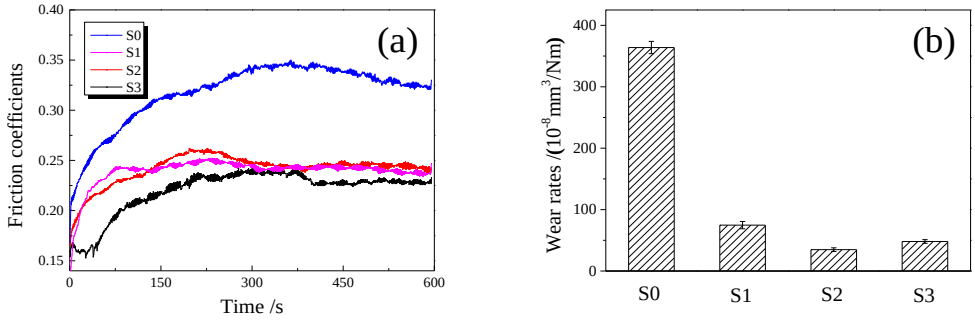

Figure 8 Friction coefficients and wear rates of the untreated surface and the composite surface under the lubrication of Ringer's solution (5 N, 5 Hz, 10 min). The composite surfaces exhibit low friction coefficients and excellent wear resistance.

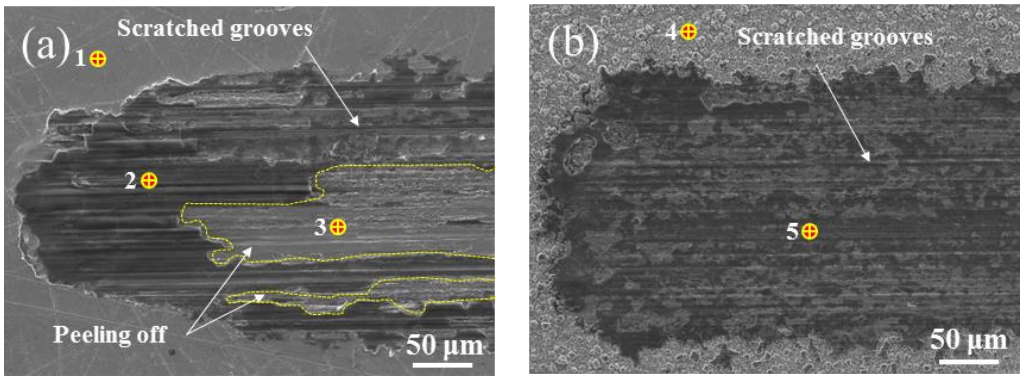

Figure 9 Morphologies of the wear tracks of (a) untreated SS surface and (b) Ag impregnated composite surface (S1), carried out within the Ringer's solution. Scratching grooves can be viewed on both untreated stainless-steel surface and the composite surface. However, peeling off areas are observed on the untreated stainless-steel surface, which implies its adhesive wear mechanism.

Table 2 EDS results for the analysed points in Figure 9 (at. %).

Point	Fe %	Ni %	Cr %	Ag %	Si %	O %
1	66.59	8.36	19.14	0	0.87	1.79
2	28.22	4.08	8.04	0	13	45.17
3	50.77	7.12	14.33	0	1.31	23.6
4	56.89	6.43	13.6	18.36	0.76	1.92
5	29.62	2.95	5.26	13.61	5.66	42.46

3.8 Antibacterial properties

The antibacterial activities of as-deposited functionally grade composite surfaces and controls against Gram-negative bacteria (*E. coli*) were investigated using a spread plate method. Colonies formed from viable *E. coli* after 5 h contact with the surfaces are shown in Figure 10. The numbers of colonies were counted to evaluate the

antibacterial activities of the surfaces while fewer colonies indicates better antibacterial performance. Figure 11 shows the counted colony forming units of *E. coli* while the stainless-steel control surfaces exhibits a low inactivation rate of *E. coli* with a high CFU number of 293.3. Besides, it was found that the antibacterial activity of the composite surfaces is related to the concentration of the impregnated Ag, while composite surface with 8 wt.% (S1) of Ag presents an average CFU of 69.5, which has a relatively lower antibacterial performance compared to the composite surfaces with more silver (15 wt.% (S2) and 25 wt.% (S3)). However, the S2 and S3 exhibit similar antibacterial performance with surviving average CFUs of 4.3 and 3, and the corresponding killing rates are 98.6% and 99%, respectively. Indicating that 5h is long enough for the contacts between the bacteria and the composite surfaces.

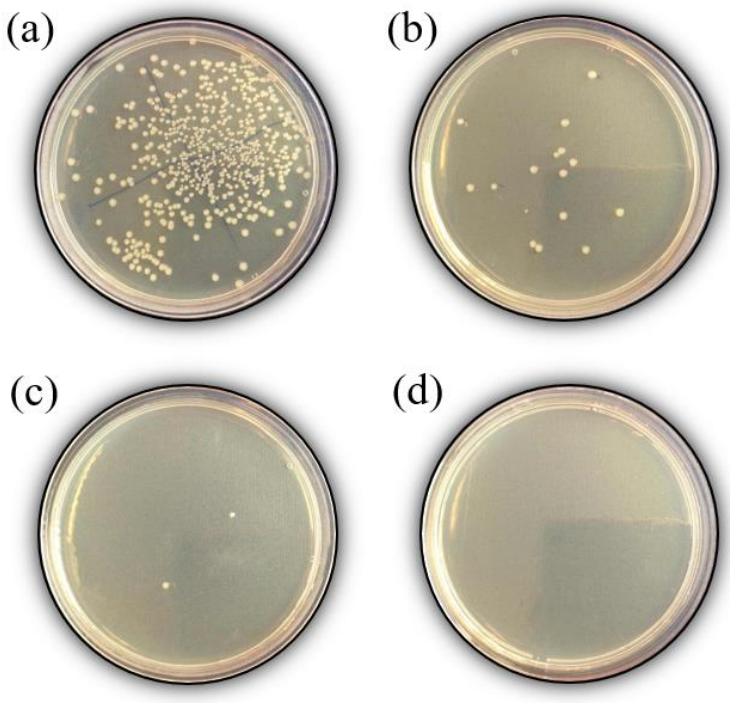

Figure 10 Colony forming units on the tryptone soya agar plates after 5 h contact with the control and functionally graded composite surfaces, the fewer colonies, the better antibacterial activity. (a) S0; (b) S1; (c) S2; (d) S3.

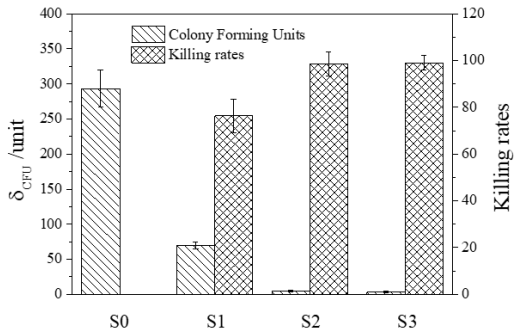

Figure 11 Average surviving number of colony forming unit δ_{CFU} (E. coli NCTC 10418) after 5 h contact with Ag impregnated composite surface and control surface.

Actually, the antibacterial process is influenced by various factors such as the content of antibacterial agents, contact time, surface roughness and so on [23]. A schematic cross-sectional image of the functionally graded surface is presented in Figure 12. The bio-functional composite surface layer is formed by sputtered Ag and stainless-steel particles, while both large and small Ag particles are generated due to the high sputtering rate of silver. Nitrogen is interacted with the stainless-steel particles and the diffusion process is caused by the concentration gradient of nitrogen. To our knowledge, the SS nanoparticles do not have antibacterial activity. Thus, the antibacterial activity of the composite surface should be attributed to the impregnated Ag particles, while the Ag particles are inert and therefore keep their antibacterial property. There are different possibilities for Ag ions to distract the biological processes of the bacteria. It was reported that Ag ions can inactivate the thiol group in enzymes to inhibit the growth of cells [44]. Besides, Choi considered that reactive oxygen species can be generated due to the existence of Ag which will damage cellular constituents and affect cell functions [45]. It is known that the antibacterial efficacy is related with the amount of Ag and the equivalent contact area [14]. As Ag is a noble metal, it is significant to design a composite surface with economical

amount of Ag which has equivalent antibacterial efficacy.

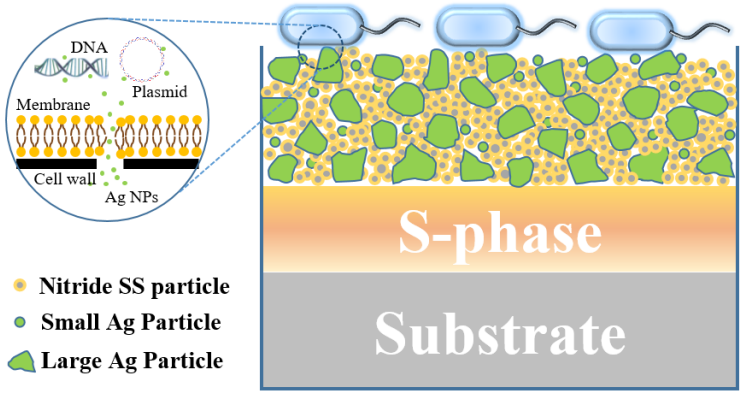

Figure 12 Schematic cross-sectional view of the functionally graded composite surface, which is formed by the bio-functional surface layer and the hard S-phase layer. The Ag ions released from the Ag particles will inhibit the growth of bacteria through the contact process.

As seen from the Figure 10 that the Ag impregnated composite surfaces present much better antibacterial activity compare to the stainless-steel surface, while composite surfaces with high percentage of Ag show higher antibacterial efficacy. To determine the statistically significant difference between these samples, a one-way analysis of variance (ANOVA) was used to understand the antibacterial performances and the multiple comparison table is shown in Table 3. The significance values between the control sample (S0) and the silver impregnated samples (S1, S2 and S3) are 0.047, 0.003 and 0.007, which are all below 0.05, indicating there are statistically significant differences of antibacterial activity between the Ag impregnated surfaces and the control surface. Besides, the results indicate there were no statistical differences of antibacterial activity between these composite surfaces after 5h contact, even though the S1 composite surface has lower antibacterial activity compares to that of the other two surfaces.

Surface roughness not only has influence on bacteria adherence, but also directly

affects the contact angle of the surface[1]. However, surface roughness plays a marginal role in these antibacterial tests. Firstly, the size of the *E. coli* NCTC 10418 is about 2 μm, which is much larger than the scale of the surface roughness. Thus, the surface roughness difference between the composite surfaces has limited effect on bacterial adherence. Besides, previous studies pointed out that typically 3-6 hour is sufficient for the fully contact between bacteria and the composite surfaces [22, 46], while 5h contact in this study is sufficient for the fully contact, which makes surface roughness a minor factor to influence the antibacterial performances of the composite surfaces.

Table 3 One-way analysis of the variance (ANOVA) of antibacterial results.

(I) Group		Mean Difference (I-J)	Std. Error	Sig.	95% Confidence interval	
					Lower Bound	Upper Bound
S0	S1	289.000*	73.398	.007	67.78	510.22
	S2	289.611*	67.003	.003	87.67	491.56
	S3	223.667*	73.398	.047	2.45	444.89
S1	S0	-289.000*	73.398	.007	-510.22	-67.78
	S2	.611	67.003	1.0	-201.33	202.56
	S3	-65.333	73.398	.851	-286.55	155.89
S2	S0	-289.611*	67.003	.003	-491.56	-87.67
	S1	-.611	67.003	1.0	-202.56	201.33
	S3	-65.944	67.003	.809	-267.89	136.00
S3	S0	-223.667*	73.398	.047	-444.89	-2.45
	S1	65.333	73.398	.851	-155.89	286.55
	S2	65.944	67.003	.809	-136.00	267.89

*. The mean difference is significant at the 0.05 level

The aim of this study was to develop long lasting functional surface with excellent antibacterial efficacy and durability. The novel duplex plasma deposition technique has obvious advantages compared to some conventional coating deposition techniques, which can fabricate a relatively thick Ag impregnated composite layer with a nitrogen

diffused hard S-phase sublayer in one step, while the percentage of Ag can be easily controlled to meet the requirements in different situation. On the other hand, the nitride stainless steel particles can act as hard reinforcements which can improve the durability of the bio-functional surface. At last, the hard S-phase sublayer provides high load bearing capacity for the composite surface which can avoid the failure caused by the soft substrate.

4. CONCLUSIONS

Functionally grade composite surfaces were developed by a novel duplex plasma alloying technique which is a synergy of double glow plasma (DGP) and active screen plasma (ASP) technologies. It has been confirmed that the Ag impregnated bio-functional surface layer combined with a hardened S-phase layer is a promising composite surface, which has excellent scratch and wear resistance, and antibacterial activity. It has been found that the applied voltages and the working distance were responsible for the microstructures of the composite surfaces, which led to the variation of the Ag particles, thickness of the S-phase layer, and surface roughness. The XRD results verified that Ag was inert during the nitriding process, and there was no reduction in antibacterial activity. The XPS peak for neutral nitrogen was detected, which indicates the S-phase stainless steel particles were formed during the nitriding process. The bottom S-phase layer improves hardness of the surface and provides high load bearing capacity, which enhanced the wear resistance of the composite surface under Ringer's solution lubricated condition. There is no statistical difference for antibacterial between the composite surfaces with different amount of Ag, and low

surviving number of Gram-negative *E. coli* remained after 5 h contact. For practical applications, the deposition parameters could be used to control the microstructures of the composite surface, and a broader spectrum of bacteria need to be further investigated to determine the optimum amount of Ag for high efficacy, long lasting bio-functional surfaces.

ACKNOWLEDGEMENT

The authors wish to express their appreciation to the financial support of the EC FIBRALSPEC project (Grant No. 604248), EC H2020-MODCOMP project (Grant No. GA685844) and National Key R&D Program of China (2017YFB0310703, 2017YFF0207905)

REFERENCES

[1] J. Hasan, R.J. Crawford, E.P. Lvanova, Antibacterial surfaces: the quest for a new generation of biomaterials, Trends Biotechnol 31(5) (2013) 31-40.

[2] K. Glinel, P. Thebault, V. Humblot, C.M. Pradier, T. Jouenne, Antibacterial surfaces developed from bio-inspired approaches, Acta Biomater 8(5) (2012) 1670-1684.

[3] S. Chernousova, M. Epple, Silver as Antibacterial Agent: Ion, Nanoparticle, and Metal, Angew Chem Int Edit 52(6) (2013) 1636-1653.

[4] F. Song, M.E. Brasch, H. Wang, J.H. Henderson, K. Sauer, D. Ren, How Bacteria Respond to Material Stiffness during Attachment: A Role of Escherichia coil Flagellar Motility, Acs Appl Mater Inter 9(27) (2017) 22176-22184.

[5] M.J. Li, L.Y. Gao, C. Schlaich, J.G. Zhang, I.S. Donskyi, G.Z. Yu, W.Z. Li, Z.X. Tu, J. Rolff,

T. Schwerdtle, R. Haag, N. Ma, Construction of Functional Coatings with Durable and Broad-Spectrum Antibacterial Potential Based on Mussel-Inspired Dendritic Polyglycerol and in Situ-Formed Copper Nanoparticles, Acs Appl Mater Inter 9(40) (2017) 35411-35418.

[6] S.H. Jeong, D.Y. Shin, I.K. Kang, E.H. Song, Y.J. Seong, J.U. Park, H.E. Kim, Effective Wound Healing by Antibacterial and Bioactive Calcium-Fluoride-Containing Composite Hydrogel Dressings Prepared Using in Situ Precipitation, Acs Biomater Sci Eng 4(7) (2018) 2380-2389.

[7] Y. Huang, X.J. Zhang, R.L. Zhao, H.H. Mao, Y.J. Yan, X.F. Pang, Antibacterial efficacy, corrosion resistance, and cytotoxicity studies of copper-substituted carbonated hydroxyapatite coating on titanium substrate, J Mater Sci 50(4) (2015) 1688-1700.

[8] A. Katsumiti, D. Gilliland, I. Arostegui, M.P. Cajaraville, Mechanisms of Toxicity of Ag Nanoparticles in Comparison to Bulk and Ionic Ag on Mussel Hemocytes and Gill Cells, Plos One 10(6) (2015).

[9] D. Campoccia, L. Montanaro, C.R. Arciola, A review of the biomaterials technologies for infection-resistant surfaces, Biomaterials 34(34) (2013) 8533-8554.

[10] X.Z. Xie, C.Y. Mao, X.M. Liu, Y.Z. Zhang, Z.D. Cui, X.J. Yang, K.W.K. Yeung, H.B. Pan, P.K. Chu, S.L. Wu, Synergistic Bacteria Killing through Photodynamic and Physical Actions of Graphene Oxide/Ag/Collagen Coating, Acs Appl Mater Inter 9(31) (2017) 26417-26428.

[11] E. Faure, C. Falentin-Daudre, T.S. Lanero, C. Vreuls, G. Zocchi, C. Van De Weerdt, J. Martial, C. Jerome, A.S. Duwez, C. Detrembleur, Functional Nanogels as Platforms for Imparting Antibacterial, Antibiofilm, and Antiadhesion Activities to Stainless Steel, Adv Funct Mater 22(24) (2012) 5271-5282.

[12] K. Vickery, D. Costa, A. Tipple, L. Lopes, H. Hu, Is it safe to continue to process stainless steel surgical instruments until functionality is compromised?, Infection, Disease & Health 22 (2017) S12.

[13] H. Qin, H.L. Cao, Y.C. Zhao, G.D. Jin, M.Q. Cheng, J.X. Wang, Y. Jiang, Z.Q. An, X.L. Zhang, X.Y. Liu, Antimicrobial and Osteogenic Properties of Silver-Ion-Implanted Stainless Steel, Acs Appl Mater Inter 7(20) (2015) 10785-10794.

[14] W. Zhang, Y.J. Luo, H.Y. Wang, J. Jiang, S.H. Pu, P.K. Chu, Ag and Ag/N(2) plasma modification of polyethylene for the enhancement of antibacterial properties and cell growth/proliferation, Acta Biomater 4(6) (2008) 2028-2036.

[15] I. Ferreri, V.S. Calderon, R.E. Galindo, C. Palacio, M. Henriques, A.P. Piedade, S. Carvalho, Silver activation on thin films of Ag-ZrCN coatings for antimicrobial activity, Mat Sci Eng C-Mater 55 (2015) 547-555.

[16] O. Sharifahmadian, H.R. Salimijazi, M.H. Fathi, J. Mostaghimi, L. Pershin, Relationship between surface properties and antibacterial behavior of wire arc spray copper coatings, Surf Coat Tech 233 (2013) 74-79.

[17] M. Roy, G.A. Fielding, H. Beyenal, A. Bandyopadhyay, S. Bose, Mechanical, In vitro Antimicrobial, and Biological Properties of Plasma-Sprayed Silver-Doped Hydroxyapatite Coating, Acs Appl Mater Inter 4(3) (2012) 1341-1349.

[18] S. Varghese, S. Elfakhri, D.W. Sheel, P. Sheel, F.J. Bolton, H.A. Foster, Novel antibacterial silver-silica surface coatings prepared by chemical vapour deposition for infection control, J Appl Microbiol 115(5) (2013) 1107-1116.

[19] Z. Xu, X. Liu, P. Zhang, Y. Zhang, G. Zhang, Z. He, Double glow plasma surface alloying

and plasma nitriding, Surf Coat Tech 201(9-11) (2007) 4822-4825.

[20] C.X. Li, T. Bell, H. Dong, A study of active screen plasma nitriding, Surf Eng 18(3) (2002) 174-181.

[21] Y.C. Dong, X.Y. Li, R. Sammons, H.S. Dong, The Generation of Wear-Resistant Antimicrobial Stainless Steel Surfaces by Active Screen Plasma Alloying with N and Nanocrystalline Ag, J Biomed Mater Res B 93b(1) (2010) 185-193.

[22] Y. Dong, X. Li, T. Bell, R. Sammons, H. Dong, Surface microstructure and antibacterial property of an active-screen plasma alloyed austenitic stainless steel surface with Cu and N, Biomed Mater 5(5) (2010).

[23] Y. Dong, X. Li, L. Tian, T. Bell, R.L. Sammons, H. Dong, Towards long-lasting antibacterial stainless steel surfaces by combining double glow plasma silvering with active screen plasma nitriding, Acta Biomater 7(1) (2011) 447-457.

[24] R. Liu, X.Y. Li, X. Hu, H.S. Dong, Surface modification of a medical grade Co-Cr-Mo alloy by low-temperature plasma surface alloying with nitrogen and carbon, Surf Coat Tech 232 (2013) 906-911.

[25] D.A. Siddiqui, S. Sivan, J.D. Weaver, M. Di Prima, Effect of wire fretting on the corrosion resistance of common medical alloys, Journal of Biomedical Materials Research Part B: Applied Biomaterials 105(8) (2017) 2487-2494.

[26] C.X. Li, T. Bell, Corrosion properties of active screen plasma nitrided 316 austenitic stainless steel, Corros Sci 46(6) (2004) 1527-1547.

[27] S. Tamilselvi, V. Raman, N. Rajendran, Corrosion behaviour of Ti-6Al-7Nb and Ti-6Al-4V ELI alloys in the simulated body fluid solution by electrochemical impedance spectroscopy,

Electrochim Acta 52(3) (2006) 839-846.

[28] S. Suzuki, S. Imai, H. Kourai, Background and evidence leading to the establishment of the JIS standard for antimicrobial products, Biocontrol science 11(3) (2006) 135-145.

[29] C. Zhao, C.X. Li, H. Dong, T. Bell, Study on the active screen plasma nitriding and its nitriding mechanism, Surf Coat Tech 201(6) (2006) 2320-2325.

[30] S.C. Gallo, H.S. Dong, On the fundamental mechanisms of active screen plasma nitriding, Vacuum 84(2) (2009) 321-325.

[31] X. Ji, X. Li, H. Yu, W. Zhang, H. Dong, Study on the carbon nanotubes reinforced nanocomposite coatings, Diam Relat Mater 91 (2019) 247-254.

[32] J.C. Stinville, P. Villechaise, C. Templier, J.P. Riviere, M. Drouet, Lattice rotation induced by plasma nitriding in a 316L polycrystalline stainless steel, Acta Mater 58(8) (2010) 2814-2821.

[33] L.C. Gontijo, R. Machado, E.J. Miola, L.C. Casteletti, N.G. Alcantara, P.A.P. Nascente, Study of the S phase formed on plasma-nitrided AISI 316L stainless steel, Mat Sci Eng a-Struct 431(1-2) (2006) 315-321.

[34] M. Esfandiari, H. Dong, Improving the surface properties of A286 precipitation-hardening stainless steel by low-temperature plasma nitriding, Surf Coat Tech 201(14) (2007) 6189-6196.

[35] X. Wang, W.T. Zheng, H.W. Tian, S.S. Yu, W. Xu, S.H. Meng, X.D. He, J.C. Han, C.Q. Sun, B.K. Tay, Growth, structural, and magnetic properties of iron nitride thin films deposited by dc magnetron sputtering, Appl Surf Sci 220(1-4) (2003) 30-39.

[36] R. Quesada-Cabrera, C. Sotelo-Vazquez, J.A. Darr, I.P. Parkin, Critical influence of

surface nitrogen species on the activity of N-doped TiO2 thin-films during photodegradation of stearic acid under UV light irradiation, Appl Catal B-Environ 160 (2014) 582-588.

[37] W.J. Gammon, O. Kraft, A.C. Reilly, B.C. Holloway, Experimental comparison of N(1s) X-ray photoelectron spectroscopy binding energies of hard and elastic amorphous carbon nitride films with reference organic compounds, Carbon 41(10) (2003) 1917-1923.

[38] T. Hanawa, S. Hiromoto, A. Yamamoto, D. Kuroda, K. Asami, XPS characterization of the surface oxide film 316L stainless steel samples that were located in quasi-biological environments, Mater Trans 43(12) (2002) 3088-3092.

[39] V. Bondarenko, S. Kaciulis, A. Plesanovas, V. Volkov, G. Zacharova, Photoelectron-Spectroscopy of the Poly-Vanadium Transition-Metal Acids, Appl Surf Sci 78(1) (1994) 107-112.

[40] H. Liu, L. Feng, J. Zhai, L. Jiang, D.B. Zhu, Reversible wettability of a chemical vapor deposition prepared ZnO film between superhydrophobicity and superhydrophilicity, Langmuir 20(14) (2004) 5659-5661.

[41] S.J. Bull, Failure Modes in Scratch Adhesion Testing, Surf Coat Tech 50(1) (1991) 25-32.

[42] M. Zouari, M. Kharrat, M. Dammak, M. Barletta, Scratch resistance and tribological performance of thermosetting composite powder coatings system: A comparative evaluation, Surface and Coatings Technology 263 (2015) 27-35.

[43] N.A. Kazerooni, M.E. Bahrololoom, M.H. Shariat, F. Mahzoon, T. Jozaghi, Effect of Ringer's Solution on Wear and Friction of Stainless Steel 316L after Plasma Electrolytic Nitrocarburising at Low Voltages, J Mater Sci Technol 27(10) (2011) 906-912.

[44] S.Y. Liau, D.C. Read, W.J. Pugh, J.R. Furr, A.D. Russell, Interaction of silver nitrate with

readily identifiable groups: relationship to the antibacterial action of silver ions, Lett Appl Microbiol 25(4) (1997) 279-283.

[45] O. Choi, Z.Q. Hu, Size dependent and reactive oxygen species related nanosilver toxicity to nitrifying bacteria, Environ Sci Technol 42(12) (2008) 4583-4588.

[46] M. Ip, S.L. Lui, V.K.M. Poon, I. Lung, A. Burd, Antimicrobial activities of silver dressings: an in vitro comparison, J Med Microbiol 55(1) (2006) 59-63.